Low Temperature Physics/Fizika Nizkikh Temperatur, 2020, vol. 46, No. 11, pp. 1253–1260

The effect of the chaotic pinning potential on intrinsic pinning in $YBa_2Cu_3O_{7-\delta}$ single crystals

N. R. Vovk[1,2], R. V. Vovk[1,3], G. Ya. Khadzhai[1], V. I. Biletskyi[1], A. V. Samoylov[1,3], A. V. Solovyov[1,4], and A. V. Matsepulin[1]

[1]*V. N. Karazin Kharkiv National University, Kharkiv 61022, Ukraine*
E-mail: rvvovk2017@gmail.com; gkhadjai@gmail.com

[2]*IFIMUP, Departamento de Fisica, Universidade de Porto, Porto 4169-007, Portugal*

[3]*Ukrainian State Academy of Railway Transport, Kharkiv 61050, Ukraine*

[4]*B. Verkin Institute for Low Temperature Physics and Engineering of the National Academy of Sciences of Ukraine Kharkiv 61103, Ukraine*

Received May 12, 2020, published online September 21, 2020

We study the temperature dependence of the in-plane magneto-resistance $\rho_{ab}(T)$ in the untwined $YBa_2Cu_3O_{7-\delta}$ single crystals after irradiation by fast electrons (energy 0.5–2.5 MeV, dose 10^{18} cm^{-2}), also with a small oxygen hypostoichiometry at different angles between the external magnetic field 15 kOe and the *ab*-planes α. We found that at high temperatures in the pseudogap region external magnetic field does not affect the $\rho_{ab}(T)$, but it broadens transitional region $T_c - T_{c0}$ from 0.3 K at zero field and $\alpha = 0$ to approximately 6 K at $\alpha = 90°$ in the field. In the case of an unirradiated sample, $\rho_{ab}(T)$ display a 3D to 2D dimensional crossover when temperature decreases from T_c to T_{c0} and scaling near the T_{c0} which we relate to the flux-flow and vortex-lattice melting. The reasons for the appearance of low-temperature "tails" (paracoherent transitions) on resistive transitions corresponding to different phase regimes of the vortex matter are discussed.

Keywords: YBaCuO single crystals, magnetoresistance, 2D–3D dimensional crossover, vortex matter, irradiation, oxygen deficiency, intrinsic pinning.

As is known irradiation with fast electrons makes it possible not only to verify the adequacy of numerous theoretical models but also to determine empirical methods for improving the technological characteristics of high-temperature superconducting cuprates (HTSC) [1, 2]. This is particularly important regarding their application [3]. From the fundamental viewpoint, it is of interest to elucidate the mechanism and degree of influence of irradiation on several unusual phenomena observed in HTSC compounds in the normal state [4, 5], such as the pseudogap anomaly [5–7], the fluctuation paraconductivity [8, 9], the incoherent electric transport [10, 11], the "metal–insulator" transitions [12, 13]. According to contemporary concepts [4, 5] these phenomena are important for understanding the microscopic nature of high-temperature superconductivity, which remains controversial, over thirty years of intense experimental and theoretical research [4–7, 14]. The precise understanding of the scattering of normal [15, 16] and fluctuational [8, 9, 14] charge carriers mechanisms, plays the most important role in these processes.

The acquisition of new functional materials with high current-carrying capacity continues to be one of the actual applied and fundamental problems of the high-temperature superconductivity physics. An important role in this is the optimization of the defective ensemble [17, 18]. As is known [19, 20], the short coherence length ξ and the large penetration depth λ lead to the fact that the pinning in HTSC becomes effective for defects such as oxygen vacancies [21] and interstitial impurities [22]. At the same time, it is often difficult to determine the degree of influence of such defects on the phase state of vortex matter due to the presence of inter-grain boundaries, twinning planes, cluster inclusions and other defects in HTSC compounds, which in turn are sufficiently robust pinning centers. The presence of "intrinsic" pinning due to the layered structure of HTSC compounds also has a significant impact [14, 21, 23].

An essential feature of $YBa_2Cu_3O_{7-\delta}$ compounds is the possibility of relatively simple obtaining of a given concentration of radiation defects relatively easily by irradiation with fast electrons [1, 2, 24]. The measurement of resistive

transitions to the superconducting state (sensitive to such a concentration) makes it possible to study the effect of radiation defects on the phase state and the dynamics of vortex matter by analyzing the fluctuation corrections to the conductivity observed in HTSC compounds at temperatures near the critical $T \approx T_c$ [21–23, 25].

In previous work [2], we investigated the effect of electron irradiation on the temperature dependence of the magnetoresistance in the region of transitions to the superconducting state of an optimally doped $YBa_2Cu_3O_{7-\delta}$ single crystal with $T_c = 91.74$ K. Here we carry out a comparative analysis of the effect of electron irradiation and a weak oxygen deficit on the temperature dependence of magnetoresistance in the region of transitions to the superconducting state.

In this paper, we investigate the effect of electron irradiation and weak oxygen deficiency on the magnetic conductivity in $YBa_2Cu_3O_{7-\delta}$ single crystals with a fixed value of the magnetic field and different values of the misorientation angle between the magnetic field vector and the direction of the basal *ab*-plane. The use of untwined single-crystal as the experimental samples allows us to exclude the effect of the inter-grain boundaries, and the chosen geometry of the experiment, to control the contribution of "intrinsic" pinning in a controlled manner.

$YBa_2Cu_3O_{7-\delta}$ single crystals were grown by the solution-melt technology in a gold crucible, according to the procedure reported previously [2]. The $YBa_2Cu_3O_{7-\delta}$ oxygen saturating regime leads to the tetra–ortho structural transition that in turn results in the crystal twinning in order to minimize its elastic energy. To obtain untwined samples, we used a dedicated chamber at 420 °C and pressured 30–40 GPa, according to the procedure of Giapintzakis *et al*. [26]. In order to obtain homogeneous controlled oxygen content, the grown crystals were annealed in an oxygen atmosphere for seven days at 420 °C.

The electrical contacts were created according to a standard 4-contact scheme by applying a silver paste on the surface of the crystal, followed by the connection of silver conductors with a diameter of 0.05 mm and three–hour annealing at a temperature of 200 °C in an oxygen atmosphere. Such a procedure allowed us to obtain a contact resistance of less than one Ohm and to conduct resistive measurements at transport currents up to 10 mA in the *ab*-plane.

In $YBa_2Cu_3O_{7-\delta}$ compounds, it is relatively easy to obtain a given concentration of point defects by varying the oxygen stoichiometry [5, 14]. To produce oxygen hypostoichiometric samples, the crystal was annealed in oxygen flow, at a temperature of 620 °C for 48 h. The measurements were performed 7 days after annealing to avoid the influence of the relaxation effects.

The measurements were carried out in the temperature drift mode with two opposite directions of the transport current to eliminate the influence of the parasitic signal. The temperature was measured with a platinum thermistor, the voltage on the sample, and the reference resistance was measured with B2-38 nanovoltmetres. The data from the voltmeters through the interface were automatically transferred to the computer. The critical temperature was determined at the maximum point on the $d\rho_{ab}(T)/dT$ dependences in the region of the superconducting transition [25].

Irradiation with electrons with energies of 0.5–2.5 MeV was carried out at temperatures $T < 10$ K. Irradiation dose $\varphi = 10^{18}$ cm^{-2} by electrons with an energy of 2.5 MeV corresponds to a concentration of defects of 10^{-4} dpa/at. at averaged over all sublattices [2]. The measurement sequence was as follows: First, we measured the temperature dependences of the samples resistance before irradiation. Then the temperature was lowered to 5 K, and irradiation was performed. The intensity of the beam was such that the temperature of the sample during irradiation did not exceed 10 K. After irradiating the sample with a dose, it was heated to 300 K and, gradually decreasing the temperature of the sample, measurements were made regarding the temperature dependences of the resistance at $T < 300$ K.

An electromagnet produced a magnetic field of up to 15 kOe. Rotating the magnet could change the orientation of the field relative to the crystal. The accuracy of the orientation of the field relative to the sample was not worse than 0.2°. The sample was mounted in the measuring cell so that the field vector **H** was always perpendicular to the transport current vector **j**.

It is well known [21, 23, 25] that the external magnetic field influences the shape of the temperature behavior of the resistance of the high-T_c cuprates nearby the superconducting transition. The transitional region broadens, and the magnetoresistance $\rho(T)$ acquires none-monotonous features which are attributed to the vortex dynamics. The temperature behavior of the in-plane magnetoresistance $\rho_{ab}(T)$ of the $YBa_2Cu_3O_{7-\delta}$ single crystals, measured at different tilt angles $\alpha \equiv \angle(H, ab)$ between the applied external magnetic field $H = 15$ kOe and the basal *ab*-planes are shown in Fig. 1. Sample in Fig. 1(a) is optimally doped with the oxygen atoms so that its critical temperature T_c at zero field $H = 0$ (curve *1*) is close to the maximal value of about 93 K at the apex of the superconducting dome. Curves *2–9* were measured in the external magnetic field $H = 15$ kOe at different tilt angles α from zero (curve *2*) up to 90° (curve *9*). All notations in Figs. 1(b) and 1(c) are the same as in Fig. 1(a). The difference is in the defects content of the samples which in Fig. 1(b) and 1(c) is more than the non-irradiated sample. That has two consequences. First, the electrical resistivity at $T = 100$ K is slightly more (51 μOhm·cm for oxygen-depleted and 64 μOhm·cm for irradiated samples) in Fig. 1(b) and Fig. 1(c) than in Fig. 1(a) where ρ_{100} it is 42 μOhm·cm, second, the shape of the curves *2–9* nearby the critical temperature are dramatically different which is more clearly seen in Fig. 2 displaying the temperature derivatives of the magnetoresistance nearby T_c, as will be discussed in more detail below.

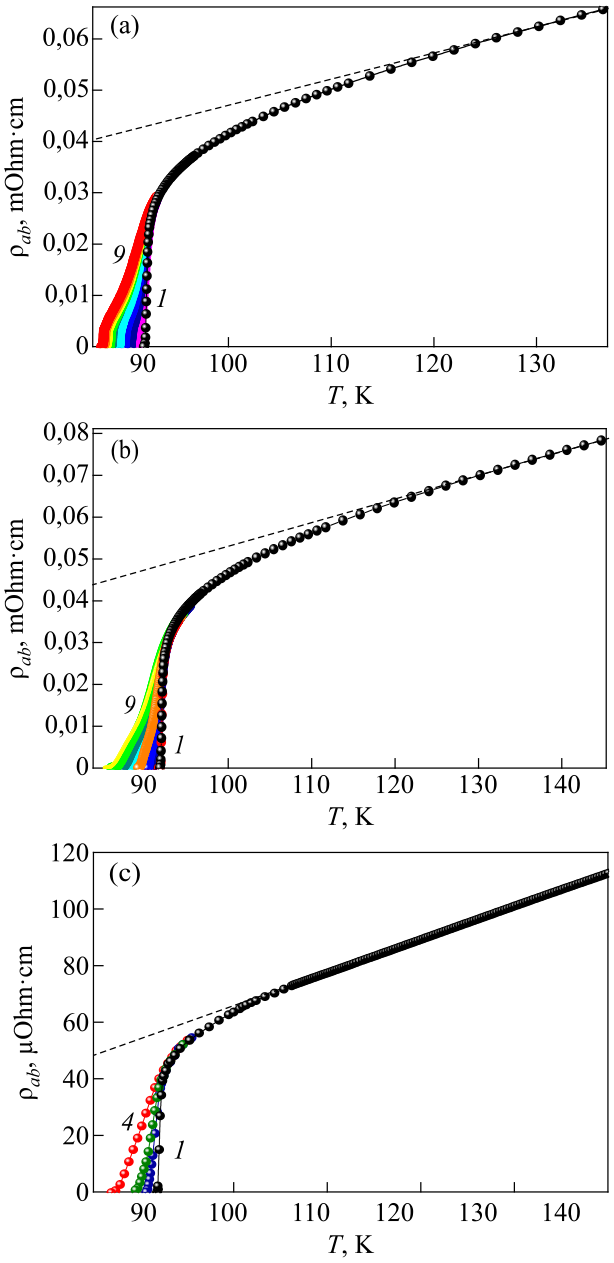

Fig. 1. (Color online) Temperature dependences of resistivity in the basal *ab*-plane, $\rho_{ab}(T)$ for the $YBa_2Cu_3O_{7-\delta}$ single crystal before (a) and after (b) lowering the oxygen content, and after irradiation (c), measured under magnetic field $H = 0$ (curve *1*) and for $H = 15$ kOe for different angles $\alpha \equiv \angle(H, ab)$: 0, 5, 10, 20, 30, 45, 60, and 90° — curves *2–9* (a), (b); 0, 14, and 90° — curves *2–4* (c), respectively. The dotted lines in the figure show a linear extrapolation of the plots in the low-temperature region.

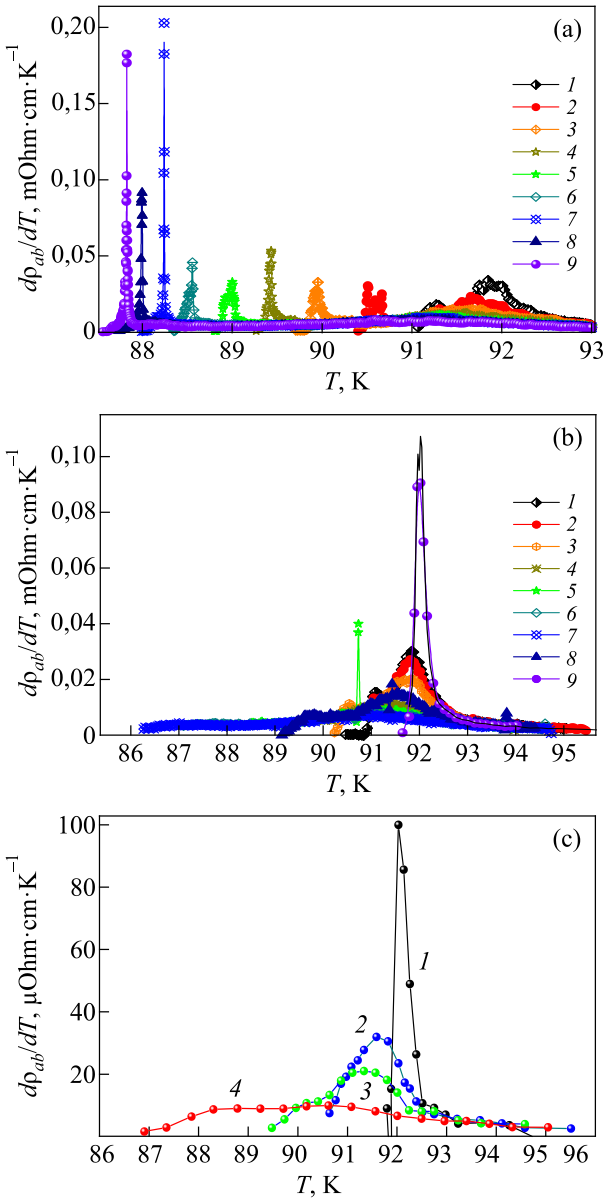

Fig. 2. (Color online) The $d\rho(T)/dT$ dependences before (a) and after (b) lowering the oxygen content, and after irradiation (c) for the $YBa_2Cu_3O_{7-\delta}$ single crystal. The numbering of the curves is consistent with Fig. 1.

The application of a magnetic field and an increase in the angle α leads to a substantial broadening of the SC transition compared with the sharp ($\Delta T_c \approx 0.3$ K) transition observed at $H = 0$ for all three samples. In this case, a significant transformation of the shape of the SC transition occurs, which is expressed in the appearance of an additional low-temperature maximum in the temperature dependences $d\rho(T)/dT$. This maximum rapidly shifts toward lower temperatures as the angle while the amplitude and width of the peak increase. It should be noted here that the aforementioned broadening of the SC transition for samples with oxygen deficiency [Fig. 1(b)] was more than three times greater than the broadening observed in the sample optimally doped with oxygen [Fig. 1(a)] at the same magnetic field and similar experimental geometry. A sharp "kink" is observed in Fig. 1(a), which is usually [21, 23, 25] explained by the manifestation of a first-order phase transition corresponding to the melting of the vortex lattice (the so-called order–disorder transition). As is known from the literature [21, 25], the presence of strong pinning centers in the system leads to a smearing of such a kink and a transition from the phase of the ordered vortex lattice to the

phase of the so-called "vortex" or "Bragg" glass, which is caused by the accommodation of the vortex system to a chaotic potential pinning. In other words, the chaotic pinning potential violates the long-range order of the vortex lattice, thereby suppressing the first-order phase transition and stimulating the realization of the glassy state of the vortices. In this case, "tails" appear on resistive junctions, the amplitude of which is less than the resistance of the viscous flow ρ_{ff}, which is probably determined by the partial pinning of the vortex fluid.

In our case, the role of such a potential can be played by clusters of oxygen vacancies. The latter assumption is supported by studies of the effect of annealing at room temperatures on excess conductivity, which we conducted for the same samples in [14]. Immediately after annealing in an oxygen atmosphere at a temperature of 500 °C, the crystal had a critical temperature $T_c \cong 91.75$ K with a transition width $\Delta T_c \cong 0.3$ K. Then the crystal was kept at room temperature for a week. As was shown in [14], this led to a decrease in the electrical resistance in the normal state $\rho(300\ \text{K})$ by ≈ 3 % and an increase in T_c by ≈ 0.25 K. Such changes are consistent with the concept of the formation of oxygen vacancy clusters during the ordering of the vacancy subsystem [5, 9, 14], which implies an increase in the oxygen concentration in the bulk of the crystal and a decrease in the oxygen content in the volume of the clusters. This leads to a decrease in the concentration of scattering centers of current carriers in the bulk of the crystal and, correspondingly, to a decrease in resistance $\rho(300\ \text{K})$. Also, taking into account the dome-shaped dependence of $T_c(\delta)$ with a maximum of $T_c \cong 93$ K at $\delta \cong 0.93$ [5, 28], we can assume that the redistribution of labile oxygen leads to phase separation in the crystal bulk and the formation of phase clusters that differ value of T_c. Given the presence of percolation paths of the current flowing through the bulk of the crystal, this process, in turn, should lead to an increase in the measured value of T_c. Thus, it can be assumed that the point pinning potential created by isolated oxygen vacancies and the pinning volume potential with a suppressed superconducting order parameter formed by clusters of oxygen vacancies coexist in the single crystal under study.

Qualitatively similar behavior of the experimental curves is also observed for a sample irradiated with fast electrons. At the same time, for this sample, the low-temperature peak in the temperature dependences $d\rho(T)/dT$, disappears almost completely, which may indicate that the "order–disorder" transition is completely suppressed. The latter, in turn, maybe due to differences in the topology of the defective ensemble in the case of oxygen-depleted and irradiated by fast electrons, which will be discussed in more detail below.

The high-temperature linear asymptotes $\rho_0 = (A + BT)$ are slightly different in Figs. 1(a) and 1(b) but the temperature $T^* \approx 134$ K where all curves merge with this asymptotes remains approximately the same. This temperature demarcates the pseudogap regime $T < T^*$ from the one in which all curves $\rho_{ab}(T)$ go down up to the some temperature near T_c where they split into a fan at different tilt angles α.

As noted above, in all cases, an external magnetic field expands the transition region. It is more convenient to analyze the transitional region in terms of conductivity $\sigma = \rho^{-1}(T)$.

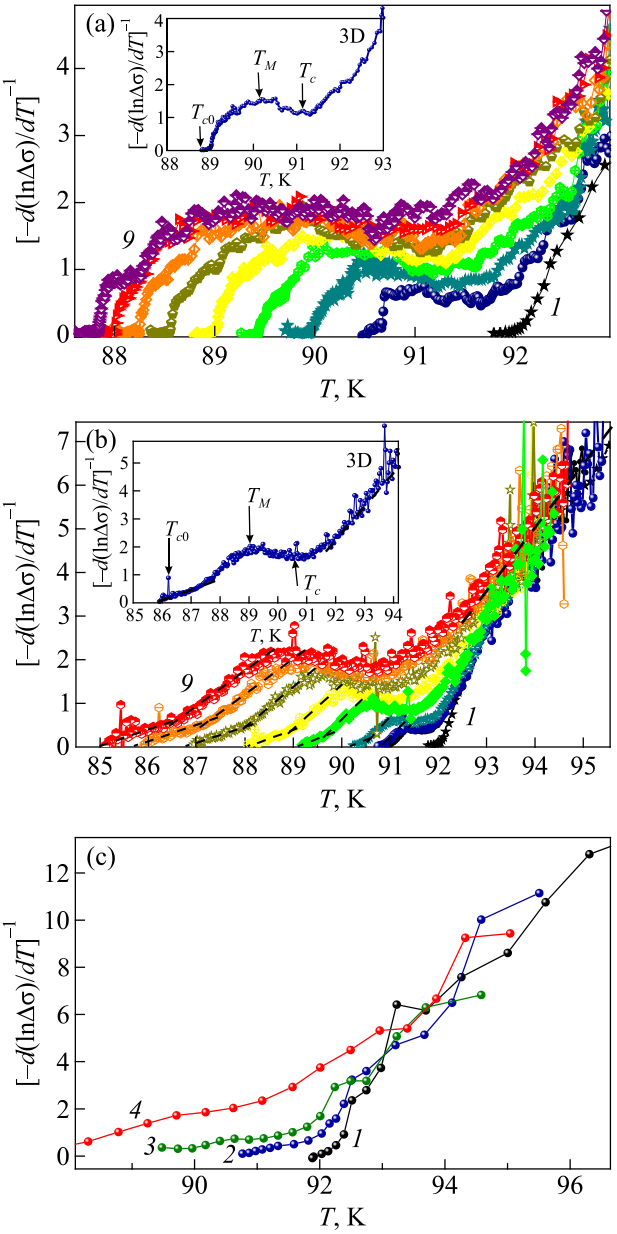

Fig. 3. (Color online) Resistivity transitions to the SC state for the $YBa_2Cu_3O_{7-\delta}$ single crystal in $\left[\frac{-d(\ln\Delta\sigma)}{dT}\right]^{-1} - T$ coordinates before (a) and after (b) lowering the oxygen content and after irradiation (c). The numbering of the curves is consistent with Fig. 1. In the insets of Fig. 3, the curve obtained for $\alpha = 60°$. The dash lines correspond to the extrapolation of the areas corresponding to various FC regimes. Arrows show the characteristic temperatures T_{c0}, T_M, and T_c, corresponding to the end of the resistive transition in SC state, the melting point of the vortex lattice and the critical temperature in the mean-field approximation, respectively.

Assuming that a deviation from the pseudogap asymptote $\sigma_0 = (A + BT)^{-1}$near the critical temperature can be written as $\Delta\sigma = \sigma - \sigma_0 \sim (T - T_c)^{-\beta}$, we plot in Fig. 3 the inverse logarithmic derivative $\chi(T) = -d \ln \Delta\sigma / dT = \beta / (T - T_c)$ at the same tilt angles of the magnetic field α as in Figs. 1 and 2. A typical curve is shown in the inserts in Fig. 3 from which one can see that the function $\chi(T)^{-1}$ has two asymptotes $\chi(T)^{-1} = \beta^{-1}{}_{c0}(T - T_{c0})$ and $\chi(T)^{-1} = \beta^{-1}{}_{c}(T - T_c)$ at temperatures T_c and T_{c0}. In this, T_{c0} is the critical temperature of the transition in para-coherent area, determined at the point of intersection with the linear interval, approximating the so-called para-coherent area with the axis of temperature. T_c is the temperature corresponding to the mean-field critical temperature, determined as the maximum in the curves $d\rho_{ab}(T)/dT$ [25]. Between these asymptotes, at the temperature T_M there is a kink that shifts towards lower temperatures and enhances its height and width with the enhancement of the tilt angle α.

Analyzing the resistive measurements in cuprates above the critical temperature in the external magnetic field it should be borne in mind that despite the nearly 35 years of intensive researches neither the nature of the charge carriers nor the mechanisms of the conductivity in cuprates are not known at the moment. Recent observation of the quantum magnetic oscillations in the underdoped cuprates [27] revealed two types of the fermion-type carriers, negatively charged "electrons" and positively charged "holes". The phase diagram of cuprates in the region of the hole concentration of our experiments $p < 0.16$ consists of the parabolic superconducting dome $T_c = T_c^{\max}[1 - 82.6(0.16 - p)^2]$ and a pseudogap crossover line $\Delta_{pg} = \Delta_{pg}^{\max}(0.27 - p)/0.22$ above it. Here p stands for a hole concentration per cuprum atom [28]. In the space between the pseudogap and the dome, at hole concentration $p < 0.16$, the Nernst effect holds which most likely is related to the vortices of unknown nature which in some theories are related to the gauge fields of the 2D strongly correlated charge carriers of cuprates [29].

The normal regime is characterized by the linear temperature resistance $\rho_0 = A + BT = \sigma_0^{-1}$ at $T > T^*$. This regime is seen clear in Fig. 1. Although below the T^* the resistance curve in Fig. 1 bends down we cannot attribute this only to the beginning of the superconducting transition since it is well known that for smaller p the resistance curve $\rho(T)$ in underdoped cuprates first upturns above ρ_0 before transition to the superconducting state at a critical temperature [30]. The physics behind this behavior is unclear so far as well as many other normal properties of cuprates.

On the other hand, the superconducting properties of cuprates are more or less the same as in conventional superconductors. Because of that, we can make some conclusions concerning the physics in the transitional region near the critical temperature is shown in Figs. 2 and 3. The broadening of the transition is in that region in the external magnetic field is caused mainly by the Abrikosov vortices. Without the magnetic field, the width of transition is small $\Delta T_c \cong 0.3$ K. In the external magnetic field in the optimally doped samples, it enhances gradually up to the value $\Delta T_c \cong 7$ K at $\alpha = 90°$ as one can see in Figs. 3(b) and 3(c). The function $\chi(T)$ in that figure has two linear asymptotes $\chi(T)^{-1} = \beta^{-1}{}_{c0}(T - T_{c0})$ and $\chi(T)^{-1} = \beta^{-1}{}_{c}(T - T_c)$ nearby the T_{c0} and T_c with $\beta_c \approx 1$ and $\beta_{c0} \approx 1/2$ which means a crossover from one regime to another when temperature decreases from T_c to T_{c0}. We argue below that this crossover can be related to the well-known 3D to 2D crossover in the upper critical field $H_{c2}(T)$ since the ratio $H / H_{c2}(T)$ determines both the flux-flow resistance $\rho_{ff}(T) = \rho H / H_{c2}(T)$ and the Abrikosov lattice elastic moduli $c_{ij} = c_{ij}[H / H_{c2}(T)]$, which are polynomials of this ratio [31]. It is well known that in layered superconductors in a tilted magnetic field, the function $H_{c2}(T)$ displays a 3D to 2D dimensional crossover [32]. This crossover is a smooth transition from the linear dependence $H_{c2}(T) \propto (T - T_c)$ just below T_c, typical for the 3D samples, to the square root dependence $H_{c2}(T) \propto (T - T_{c0})^{1/2}$ which holds in 2D thin layers. A nontrivial feature of this 3D to 2D crossover is that the temperature T_{c0} is lower than the T_c. As was shown in the papers [33, 34] the difference $T_c - T_{c0}$ depends on the strength and some other details of the coupling between the layers.

The resistance $\rho_{ab}(T) = \rho_0(1 + \Delta\sigma\rho_0)^{-1}$near the transition is determined by the term $\Delta\sigma\rho_0$ which means that singularities in the $\rho_{ab}(T)$ are of the same nature as in the $\Delta\sigma(T)$. (In case $\Delta\sigma\rho_0 << 1$ the quantity $\Delta\rho_{ab} = \rho_{ab} - \rho_0$ can be written as $\Delta\rho_{ab} \approx -\rho_0^2\Delta\sigma$). In optimally doped untwined single crystals there are no pinning centers that may fixe or distort the Abrikosov lattice. Under such circumstances, it is natural to assume that the resistance near the transition temperature in our experiments is due to the flux-flow mechanism which contributes to the $\rho_{ab}(T)$ is given by the formula $\rho_{ff}(T, \alpha) = \rho H^{\text{perp}}(\alpha) / H_{c2}(T)$. For fixed tilt angle α the value of $H^{\text{perp}}(\alpha)$ is constant and the temperature behavior of the flux-flow resistance completely depends on the $H_{c2}(T)$ which grows up and displays 3D to 2D crossover with the decrease of temperature. Therefore the $\rho_{ff}(T, \alpha)$ decreases as a function of temperature and displays near the superconducting transition the same 3D to 2D crossover as that observed in the function $\Delta\sigma(T)$. Approximating the value of the resistance decrease near the transition $|\Delta\rho_{ab}| \approx \Delta\sigma\rho_0^2$ by the flux-flow resistance $\rho_{ff}(T, \alpha)$ we can explain the crossover in $\Delta\sigma(T)$ and related asymptotes $\chi(T)^{-1} = \beta^{-1}{}_{c0}(T - T_{c0})$ and $\chi(T)^{-1} = \beta^{-1}{}_{c}(T - T_c)$ by the 3D to 2D crossover in the upper critical field $H_{c2}(T)$ and in the $\rho_{ff}(T, \alpha)$. With the enhancement of the tilt angle α a perpendicular to layers component of the external magnetic field $H^{\text{perp}}(\alpha)$ and $\rho_{ff}(T, \alpha)$ increase in agreement with our observations. The kink between the asymptotes is related to the transitional region of the 3D to 2D crossover. This crossover through the elastic moduli of the Abrikosov lattice $c_{ij} = c_{ij}[H / H_{c2}(T)]$ has also an impact on the melting line [35]. The melting

line $H_M(T)$ goes below the $H_{c2}(T)$ on the phase diagram and in the absence of the pinning centers depends on the shape of the $H_{c2}(T)$. The flux-flow resistances of the melted and regular Abrikosov lattices are different. The melted Abrikosov lattices are in a disordered glassy state for which as was shown in [25], the function $\chi(T)$must display scaling in some reduced coordinates. The corresponding plot is given in Fig. 4 for the irradiated and oxygen-deficient sample. It displays a scaling close to the temperature T_{c0}. This will be discussed in more detail below.

Deviation from the optimal doping after irradiation towards the underdoped region $p < 0.16$ brings oxygen vacancies into the *ab*-planes which are effective pinning centers in cuprates. A pinned Abrikosov lattices are distorted and do not flow. The resistance, in that case, is due to the hopping of the vortices, and 3D to 2D crossover is absent. That explains a dramatic difference between the pictures in Figs. 2(a)–2(c).

Applying magnetic field and increasing the angle α lead to a significant transformation of the shape of the SC transition, which is expressed in the appearance of an additional low-temperature maximum, of the so-called "paracoherent transition" [25]. There is a noticeable difference in the behavior of this maximum in the case of oxygen-deficient and irradiated and unirradiated samples. While for an unirradiated sample this transition shifts toward low temperatures, practically unchanging its shape, in the second and third cases such a shift is accompanied by a significant elongation of the "low-temperature tail" of the superconducting transition by the increase of angle α. Such a behavior can be caused by a decrease of the fraction of intrinsic pinning with increasing α and, correspondingly, an increase in the role of volume pinning due to the formation of strong pinning centers in the bulk (volume) of the sample itself.

As it is known from the bibliography [21 ,23, 25, 36, 37], the presence of strong pinning centers in the system leads to a blurring of the above-mentioned kink and to a transition from the phase of the ordered vortex lattice to the so-called "Bragg glass" phase, which is due to the accommodation of the vortex system to a chaotic pinning potential. In other words, the chaotic pinning potential disrupts the long-range order of the vortex lattice, thereby suppressing the first-order phase transition and stimulating the realization of the glass state of the vortices. Thus, extended "tails" appear on the resistive transitions, the amplitude of which is smaller than the resistance of the viscous flow ρ_{ff}, which is probably determined by partial pinning of the vortex liquid. In our case, the radiation defects could play the role of such potential. The latter assumption is supported by studies regarding the influence of irradiation with fast electrons on the excess conductivity, carried out for the same samples in [2]. Immediately after irradiating the crystal at temperatures $T < 10$ K, the width of the superconducting transition ΔT_c increased almost twofold. Herewith, irradiation led to an increase in the electrical resistance in the normal state ρ(300 K) by ≈ 67 %, and the ratio ρ(300 K)/ρ(0 K) decreased from 40 to 14. Such changes indicate a significant increase in the concentration of the carrier's scattering effective centers in the bulk of the crystal. Thus, it can be assumed that in the investigated single-crystal exists point pinning potential, created by isolated oxygen vacancies, and a pinning volume potential with a suppressed superconducting order parameter formed by radiation defects.

As it was determined by Costa *et al.* [25], in the case of the realization of the "Bragg glass" state in the system on the $\chi(T)$ curves, a scaling should be observed in the reduced coordinates $\chi(T_c - T_{c0}) - (T - T_{c0})/(T_c - T_{c0})$, where T_{c0} is the critical temperature of the end of the transition in the paracoherent region, determined at the intersection point of the linear section, approximating the so-called paracoherent region, with the temperature axis, where T_c is the temperature corresponding to the mean-field critical temperature, determined at the maximum point on the $d\rho_{ab}(T)/dT$ curves [23, 25].

Figure 4 shows the same curves scaled as $\chi(T_c - T_{c0})/\varepsilon_\alpha - (T - T_{c0})/(T_c - T_{c0})$. Herewith, we considered the change

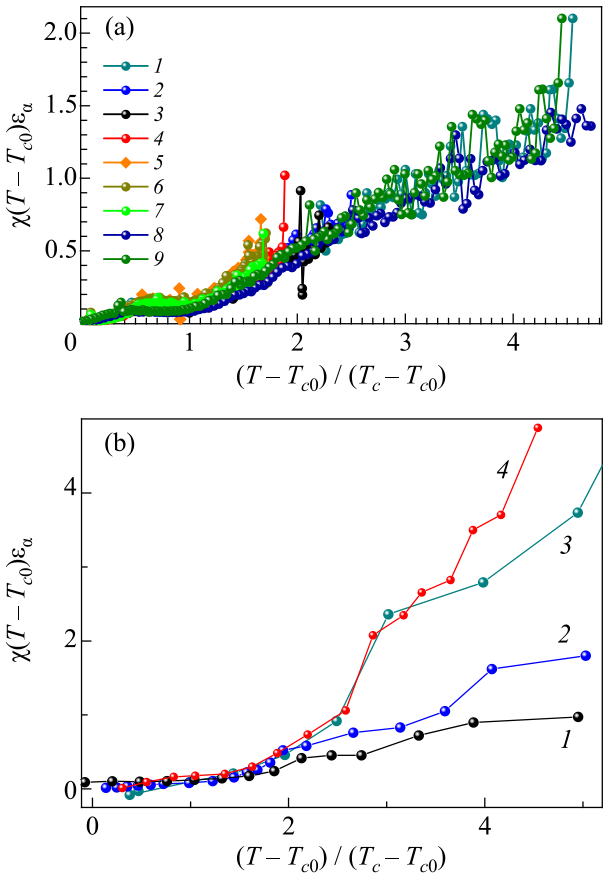

Fig. 4. (Color online) Resistivity transition to the SC state in the basal *ab*-plane $\rho_{ab}(T)$ after lowering the oxygen content (a) and after irradiation (b) for the $YBa_2Cu_3O_{7-\delta}$ crystal in (reducing) $\chi(T_c - T_{c0})/\varepsilon_\alpha - (T - T_{c0})/(T_c - T_{c0})$ coordinates. The numbering of the curves is consistent with Fig. 1.

in the contribution of the intrinsic pinning by increasing the misorientation angle $\alpha \equiv \angle(H, ab)$, by adjusting the value of $\chi(T_c - T_{c0})$ taking into account the anisotropy parameter [23, 37] $\varepsilon_\alpha = (\sin^2\alpha + \varepsilon^2\cos^2\alpha)^{1/2}$, where ε = 6–9. As it can be seen from Fig. 4, the experimental curves, the best scaling is observed in the paracoherent region at $T < T_M$. At higher temperatures, the scatter of the curves becomes more substantial, apparently, as a result of the pinning of the superconducting fluctuations on radiation defects, and also the possible enhancement of the role of certain specific mechanisms of quasiparticle interaction [38–43]. It should be noted that the differences in the behavior of the dependencies $\chi(T_c - T_{c0})/\varepsilon_\alpha - (T - T_{c0})/(T_c - T_{c0})$, observed for oxygen-deficient and irradiated samples. While in the first case scaling is observed over the entire temperature range of resistive transitions to the superconducting state, in the second case scaling is observed only in the low-temperature part for $(T - T_{c0})/(T_c - T_{c0}) < 2$. As noted above, this behavior may be due to differences in the topology of the defects ensemble in the case of oxygen-depleted and irradiated by fast electrons. The distribution of oxygen clusters in the volume of the experimental sample is apparently quite isotropic, as evidenced, for example, by the results of [14, 20]. At the same time, the distribution of radiation defects that form in the crystal under study upon irradiation with fast electrons according to our technique probably has a much greater degree of anisotropy than in the previous case. This is primarily due to the distinguished direction of electron irradiation perpendicular to the base *ab*-plane of the crystal, [24] as well as to the fact that the irradiation itself was carried out at temperatures near the temperature of liquid helium and without additional annealing of the sample [2]. Apparently, the latter contributed to the "freezing" of the obtained distribution of radiation defects due to the slowdown of their diffusion movement in the volume of the experimental sample.

In conclusion, we found that in optimally doped untwined single crystals YBaCuO: (i) The function $\chi(T)$ has a linear asymptotes $\chi(T)^{-1} = \beta^{-1}{}_{c0}(T - T_{c0})$ and $\chi(T)^{-1} = \beta^{-1}{}_{c}(T - T_c)$ nearby the T_{c0} and T_c with $\beta_c \approx 1$ and $\beta_{c0} \approx 1/2$. (ii) We relate this with the well-known 3D to 2D crossover in the upper critical field $H_{c2}(T)$ in the layered superconductors, which through the ratio $H / H_{c2}(T)$ influences the flux-flow resistance and the melting line of the Abrikosov vortex-lattice. (iii) The width of the transitional region $T_c - T_{c0}$ increases from 0.3 K at zero field and $\alpha = 0$ to approximately 6 K at α = 90°. (iv) In case unirradiated sample, the function $\chi(T)$ displays a universal form with maximum near the temperature T_M, which means melting of the Abrikosov vortex-lattice. (v) In case of irradiated and oxygen-deficient samples at temperatures below the critical $T < T_c$, there is a suppression of the dynamic phase transition type liquid vortex–vortex lattice and formation in the system of a transition type liquid vortex–vortex "Bragg" glass.

1. F. Rullier-Albenque, H. Alloul, and R. Tourbot, *Phys. Rev. Lett*. **91**, 047001 (2003).
2. V. I. Beletskiy, G. Ya. Khadzhai, N. R. Vovk, Yu. V. Litvinov, V. V. Sklyar, and I. L. Goulatis, *Funct. Mater*. **26**, 477 (2019).
3. S. I. Bondarenko, V. P. Koverya, A. V. Krevsum, and S. I. Link, *Fiz. Nizk. Temp.* **43**, 1482 (2017). [*Low Temp. Phys*. **43**, 1125 (2017)].
4. J. Ashkenazi, *Supercond. Nov. Magn*. **24**, 1281 (2011).
5. R. V. Vovk and A. L Solovyov, *Fiz. Nizk. Temp*. **44**, 111 (2018) [*Low Temp. Phys*. **44**, 81 (2018)].
6. A. A. Kordyuk, *Fiz. Nizk. Temp*. **41**, 417 (2015) [*Low Temp. Phys*. **41**, 319 (2015)].
7. R. V. Vovk, A. A. Zavgorodniy, M. A. Obolenskii, I. L. Goulatis, A. Chroneos, and V. M. Pinto Simoes, *Modern Phys. Lett. B* **24**, 2295 (2010).
8. T. A. Friedmann, J. P. Rice, J. Giapintzakis, and D. M. Ginsberg, *Phys. Rev. B* **39**, 4258 (1989).
9. A. L. Solovjov, L. V. Omelchenko, R. V. Vovk, O. V. Dobrovolskiy, Z. F. Nazyrov, S. N. Kamchatnaya, and D. M. Sergeyev, *Physica B* **493**, 58 (2016).
10. R. V. Vovk, M. A. Obolenskii, A. A. Zavgorodniy, I. L. Goulatis, A. I. Chroneos, and V. M. Pinto Simoes, *J. Mater. Sci: Mater. Electron.* **20**, 858 (2009).
11. R. V. Vovk, M. A. Obolenskii, A. A. Zavgorodniy, A. V. Bondarenko, I. L. Goulatis, A. V. Samoilov, A. I. Chroneos, and V. M. Pinto Simoes, *J. Alloys Comp.* **464**, 58 (2008).
12. K. Widdera, D. Bernera, H. P. Geserich, W. Widder, and H. F. Braun, *Physica C* **251**, 274 (1995).
13. R. V. Vovk, Z. F. Nazyrov, I. L. Goulatis, and A. Chroneos, *Physica C* **485**, 89 (2013).
14. A. L. Solovjov, E. V. Petrenko, L. V. Omelchenko, R. V. Vovk, I. L. Goulatis, and A. Chroneos, *Scientific Rep*. **9**, 9274 (2019).
15. R. V. Vovk, N. R. Vovk, G. Ya. Khadzhai, I. L. Goulatis, and A. Chroneos, *Solid State Commun*. **190**, 18 (2014).
16. R. V. Vovk, N. R. Vovk, G. Ya. Khadzhai, Oleksandr V. Dobrovolskiy, and Z. F. Nazyrov, *J. Mater. Sci: Mater. Electron*. **25**, 5226 (2014).
17. O. V. Dobrovolskiy, M. Huth, V. A. Shklovskij, and R. V. Vovk, *Scientific. Rep.* **7**, 13740 (2017).
18. A. L. Solovjov, L. V. Omelchenko, E. V. Petrenko, R. V. Vovk, V. V. Khotkevych, and A. Chroneos, *Scientific Rep.* **9**, 20424 (2019).
19. G. Blatter, M. V. Feigel'man, V. B. Geshkenbein, and V. M. Vinokur, *Rev. Mod. Phys*. **66**, 1125 (1994).
20. A. V. Bondarenko, V. A. Shklovskij, M. A. Obolenskii, R. V. Vovk, A. A. Prodan, M. Pissas, D. Niarchos, and G. Kallias, *Phys. Rev. B* **58**, 2445 (1998).
21. W. K. Kwok, S. Fleshier, U. Welp, V. M. Vinokur, J. Downey, G. W. Cratree, and M. M. Miller, *Phys. Rev. Lett.* **69**, 3370 (1992).
22. R. V. Vovk, M. A. Obolenskii, A. A. Zavgorodniy, Z. F. Nazyrov, I. L. Goulatis, V. V. Kruglyak, and A. Chroneos, *Modern Phys. Lett. B* **25**, 2131 (2011).

23. R. V. Vovk, Z. F. Nazyrov, M. A. Obolenskii, I. L. Goulatis, A. Chroneos, and V. M. P. Simoes, *J. Alloys Comp*. **509**, 4553 (2011).
24. G. Ya. Khadzhai, R. V. Vovk, Z. F. Nazyrov, and O. V. Dobrovolskiy, *Physica C* **565**, 1353507 (2019).
25. R. M. Costa, I. C. Riegel, A. R. Jurelo, and J. L. Pimentel, *J. Magn. Magn. Mater*. **320**, 493 (2008).
26. J. Giapintzakis, D. M. Ginzberg, and P. D. Han, *J. Low Temp. Phys*. **77**, 155 (1989).
27. N. Doiron-Leyraud, C. Proust, D. LeBoeuf, J. Levallois, J.-B. Bonnemaison, R. Liang, D. A. Bonn, W. N. Hardy, and L. Taillefer, *Nature* **447**, 565 (2007).
28. S. Hufner, M. A. Hossail, A. Domascelli, and G. A. Sawatsky, *Rep. Prog. Phys*. **71**, 062501 (2008).
29. P. A. Lee, N. Nagaosa, and X. G. Wen, *Rev. Mod. Phys*. **78**, 17 (2006).
30. A. A. Zavgorodniy, R. V. Vovk, M. A. Obolenskii, and A. V. Samoilov, *Fiz. Nizk. Temp.* **36**, 143 (2010) [*Low Temp. Phys*. **36**, 115 (2010)].
31. E. H. Brandt, *Phys. Rev. B* **34**, 6514 (1986).
32. B. Y. Jin and J. B. Ketterson, *Adv. Phys.* **38**, 189 (1989).
33. V. M. Gvozdikov, *Fiz. Nizk. Temp*. **16**, 1156 (1990) [*Sov. J. Low Temp. Phys*. **16**, 668 (1990)].
34. V. M. Gvozdikov and M. Teixeira, *Fiz. Nizk. Temp*. **19**, 1302 (1993) [*Low Temp. Phys*. **19**, 922 (1993).
35. V. M. Gvozdikov and L. Z. Kaganovsky, *Czech. J. Phys*. **46**, 1181 (1996).
36. A. V. Bondarenko, V. A. Shklovskij, R. V. Vovk, M. A. Obolenskii, and A. A. Prodan, *Fiz. Nizk. Temp*. **19**, 1281 (1997) [*Low Temp. Phys*. **19**, 962 (1997)].
37. A. V. Bondarenko, A. A. Prodan, M. A. Obolenskii, R. V. Vovk, and T. R. Arouri, *Fiz. Nizk. Temp*. **27**, 463 (2001) [*Low Temp. Phys*. **27**, 339 (2001)].
38. R. V. Vovk, C. D. H. Williams, and A. F. G. Wyatt, *Phys. Rev. B* **69**, 144524 (2004).
39. D. H. S. Smith, R. V. Vovk, C. D. H. Williams, and A. F. G. Wyatt, *Phys. Rev. B* **72**, 054506 (2005).
40. O. V. Dobrovolskiy, V. M. Bevz, M. Yu. Mikhailov, O. I. Yuzephovich, V. A. Shklovskij, R. V. Vovk, M. I. Tsindlekht, R. Sachser, and M. Huth, *Nature Commun*. **9**, 4927 (2018).
41. O. V. Dobrovolskiy, R. Sachser, T. Brächer, T. Fischer, V. V. Kruglyak, R. V. Vovk, V. A. Shklovskij, M. Huth, B. Hillebrands, and A. V. Chumak, *Nature Phys.* **15**, 477 (2019).
42. M. A. Hadi, M. Roknuzzaman, A. Chroneos, S. H. Naqib, A. K. M. A. Islam, R. V. Vovk, and K. Ostrikov, *Comput. Mater. Science* **137**, 318 (2017).
43. N. Kuganathan, P. Iyngaran, R. Vovk, and A. Chroneos, *Scientific. Rep*. **9**, 4394 (2019).

Вплив хаотичного потенціалу пінінгу на власний пінінг у монокристалах $YBa_2Cu_3O_{7-\delta}$

М. Р. Вовк, Р. В. Вовк, Г. Я. Хаджай, В. І. Білецький, О. В. Самойлов, А. Л. Соловйов, А. В. Мацепулін

Досліджено температурну залежність магнітоопору в площині шарів у бездвійникових монокристалах $YBa_2Cu_3O_{7-\delta}$ після опромінення швидкими електронами (енергія 0,5–2,5 МеВ, доза 10^{18} см$^{-2}$), а також з невеликою кисневою гіпостехіометрією під різними кутами між зовнішнім магнітним полем 15 кЕ та *ab*-площиною. Виявлено, що при високих температурах в області псевдощілинного стану магнітне поле не впливає на залежності $\rho_{ab}(T)$, але воно розширює надпровідний перехід від 0,3 К без поля до приблизно 6 К при $\alpha = 90°$ у полі. У випадку неопроміненого зразка $\rho_{ab}(T)$ демонструє розмірний 3D–2D кросовер при зниженні температури від T_c до T_{c0} та скейлінг поблизу T_{c0}, який пов'язано з в'язкою течією потоку та плавленням вихрової решітки. Обговорюються причини появи низькотемпературних «хвостів» (паракогерентних переходів) на резистивних переходах, що відповідають різним фазовим режимам вихрової матерії.

Ключові слова: монокристали YBaCuO, магнітоопір, 2D–3D розмірний кросовер, вихрова матерія, опромінення, дефіцит кисню, власний пінінг.